# Large-Strain, Multiform Movements from Designable Electrothermal Actuators Based on Large Highly Anisotropic Carbon Nanotube Sheets

**Qingwei Li,*,† Changhong Liu,*,† Yuan-Hua Lin,‡ Liang Liu,† Kaili Jiang,† and Shoushan Fan†**

†Tsinghua-Foxconn Nanotechnology Research Center and Department of Physics and ‡School of Materials Science and Engineering, Tsinghua University, Beijing 100084, China

**ABSTRACT** Many electroactive polymer (EAP) actuators use diverse configurations of carbon nanotubes (CNTs) as pliable electrodes to realize discontinuous, agile movements, for CNTs are conductive and flexible. However, the reported CNT-based EAP actuators could only accomplish simple, monotonous actions. Few actuators were extended to complex devices because efficiently preparing a large-area CNT electrode was difficult, and complex electrode design has not been carried out. In this work, we successfully prepared large-area CNT paper (buckypaper, BP) through an efficient approach. The BP is highly anisotropic, strong, and suitable as flexible electrodes. By means of artful graphic design and processing on BP, we fabricated various functional BP electrodes and developed a series of BP—polymer electrothermal actuators (ETAs). The prepared ETAs can realize various controllable movements, such as large-stain bending (>180°), helical curling (~630°), or even bionic actuations (imitating human-hand actions). These functional and interesting movements benefit from flexible electrode design and the anisotropy of BP material. Owing to the advantages of low driving voltage (20—200 V), electrolyte-free and long service life (over 10000 times), we think the ETAs will have great potential applications in the actuator field.

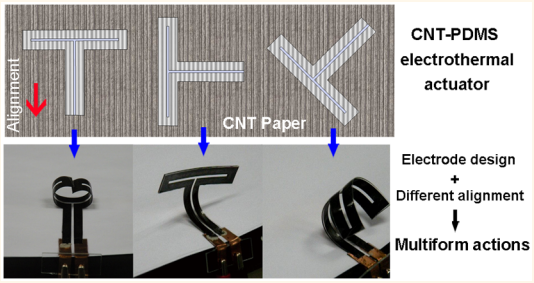


**KEYWORDS:** electrothermal actuators · multiform movements · carbon nanotubes · anisotropy · electrode design

As technology develops, new requirements are raised for actuators as bionic robots, flexible lens focusing, dynamic braille display, *etc.*, which require discontinuous, agile, and complex actions. Conventional actuators (combustion engine, electromotor, piezoelectric ceramic) cannot meet these demands.[1] So the scientists have been developing new actuators. The electroactive polymer (EAP) actuators have gradually become mainstream because they can achieve large-strain discontinuous actuations driven by electrical field or current and have the advantages of easy control and low cost.[2−4] The EAP actuators are usually based on flexible electrodes and polymers, and they can be classified as several types, such as electronic actuators, ionic actuators, *etc.*[3,4] The electronic actuators employ ultrahigh electric fields to realize electrode interattraction (dielectric actuators)[4−7] or to make configurations of the microscopic charged objects (dipoles and polar molecule chains or groups) changed or realigned (such as electrostrictive polymers, ferroelectrive elastomers, and liquid crystal elastomers).[8,9] The field-driven actuation mechanism inevitably results in ultrahigh driving voltage (over 1000 V). The ionic EAP actuators, by contrast, only need low voltage (<10 V) to drive ions in the polymer phase to make certain regions of the polymer swell or contract, so that the actuator extends or bends.[10−13] It is essential, however, to maintain a "wet" electrolyte environment. Until now, the ultrahigh driving voltage and indispensable electrolyte environment controlled the electronic[5,6] and ionic EAP actuators.[12−14]

In recent years, electrothermal actuators (ETAs) have emerged as an important branch of EAP actuators because they have

* Address correspondence to liqingwei@tsinghua.org.cn, chliu@mail.tsinghua.edu.cn.

Received for review September 29, 2014 and accepted January 5, 2015.

**Published online January 05, 2015**
**10.1021/nn505535k**

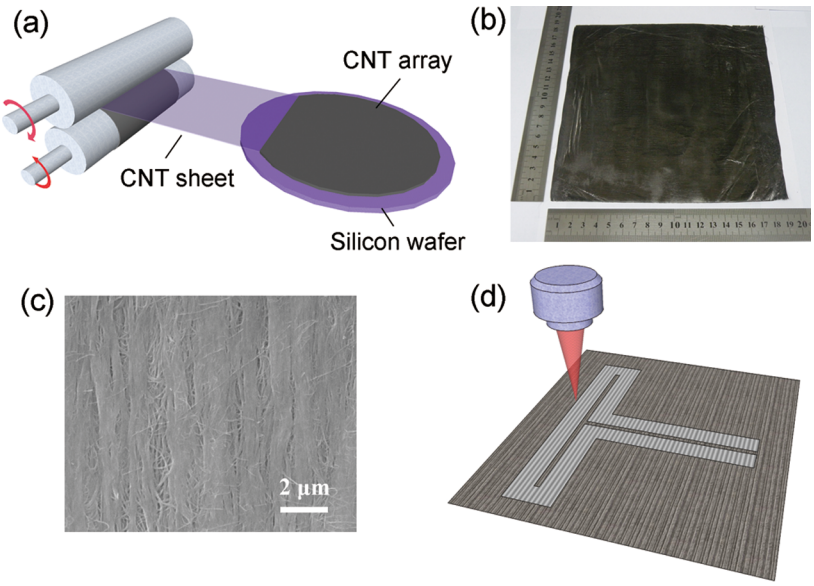


**Figure 1. Preparation of BP and processing on it. (a) Schematic of preparing BP: the continuous CNT sheet was drawn from a superaligned CNT array and rolled up by two cylindrical steel rollers to make compact BP. (b) Photograph of the as-prepared BP. (c) Scanning electron microscope image of the as-prepared BP where the CNTs are all well aligned in one direction neatly. (d) Schematic of graphic design and laser cutting on BP to make a T-shaped conductive band.**

low driving voltage and are electrolyte free.[15−20] The ETAs are flexible devices based on pliable electrodes and polymers and can carry out large deformations by current or light heating.[15,18−22] Throughout the literature, the ETAs are of two types. One is a uniform conductive composite film that can expand or contract with a rise or drop in temperature.[15−17] The other type is a double-layer composite film that is made of a flexible electrode and polymer with a great difference in coefficient of thermal expansion (CTE).[18−22] When current or light heated, the double-layer actuator could bend to the side that has smaller thermal expansion.

Strong, flexible electrode materials are indispensable in preparing EAP actuators. Carbon nanotube (CNT) is one of the best candidates for electrode material because it is conductive and flexible and has excellent thermal and chemical stability.[23−27] Many EAP actuators use diverse configurations of CNT as flexible electrodes to realize discontinuous, agile movements.[10,15−21,28−32] However, the reported CNT-based EAP actuators had very simple structures and designs, *e.g.*, a thread of CNT-polymer composite[15−17] or a strip consisting of several layers of different materials.[18−20] These actuators could only accomplish simple, monotonous movements which are far from practical applications. In addition, few actuators have been developed to complex devices. This is because efficiently preparing a large-area CNT-based electrode is still a difficult task, and consequently, complex electrode designs could not be carried out easily.

In this work, we introduce an efficient approach to prepare a large-area CNT paper (buckypaper, BP) that is strong, highly anisotropic, and suitable as a flexible electrode. Based on this large-area anisotropic BP material, we carried out graphic design and efficient processing to obtain a series of functional flexible electrodes and developed various CNT−polymer double-layer ETAs. Under electrical heating, the prepared ETAs can realize multiform controllable movements, such as large-stain bending (>180°), helical curling (~630°), or even bionic actuation (imitating human-hand actions). The ETAs also have the advantages of having low driving voltage (20 V − 200 V), being electrolyte free, and having long service life (over 10000 times).

## RESULTS AND DISCUSSION

**Preparation of Large-Area BP and Various Well-Designed ETAs.** The large-area BP is made of 1000 layers of CNT sheets drawn from a superaligned CNT array. In our laboratory, we have developed a set of mature technologies to produce superaligned CNT arrays on 8-in. silicon wafers in large batch which were described elsewhere.[33−36] The continuous CNT sheet drawn from the CNT array was rolled up by two cylindrical steel rollers with high speed. We then cut it up and spread it to form an 18 cm-square compact paper with a thickness of 40−50 $\mu$m as shown in Figure 1a,b. The prepared BP is conductive, strong, and suitable as flexible electrode material. Thus, massive and efficient production of a large-area CNT electrode is technically feasible. On this large-area paper, carrying out complex design and fine processing are also viable. In addition, the CNTs of BP are all well aligned in one direction neatly, as revealed by the scanning electron microscope image (Figure 1c), so the BP material shows obvious anisotropic properties. The electrical conductivity along the CNT aligned direction is about

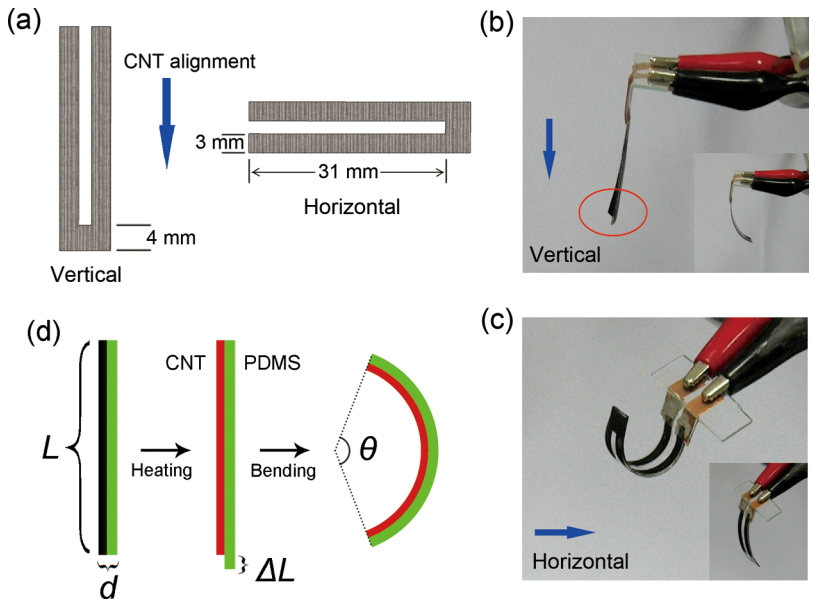


**Figure 2. Actuations of the U-shaped ETAs and the actuation mechanism. (a) Schematic of vertically cut and horizontally cut U-shaped BP electrodes. (b, c) Actuations of the U-shaped ETAs with vertical and horizontal CNT alignment. The blue arrows indicate the CNT aligned direction. Insets: original shapes of the ETAs before current heating. (d) Schematic illustration of electrothermal actuation mechanism for CNT-PDMS double-layer ETA. The middle configuration where the two straight layers have different lengths does not exist in reality. Instead, the composite film would bend to BP side when electrically heated.**

$3 \times 10^4$ S m$^{-1}$, which is one magnitude larger than that perpendicular to the CNT alignment. The density of the prepared BP is about $0.8 \pm 0.1$ g/cm$^3$. The fluctuations in density will have a little influence on the electrical and thermal conductivity of BP and further the heat generation and temperature distribution of the actuator. But these small changes caused by density fluctuation would not bring significant impact on the actuation performances of the ETAs.

On the large-area BP, we then carried out complex graphic design and laser cutting to get functional patterns of BP bands as electrodes, for example, a T-shaped band as shown in Figure 1d. After several processes, the ETA could be made. For detailed information, see the Methods and video S1 (Supporting Information). The prepared ETA is a double-layer composite film made of BP and heat-resistant polydimethylsiloxane (PDMS).[37] By virtue of artful electrode design and the superior properties of BP, the as-prepared ETAs can accomplish interesting multiform deformations.

**U-Shaped ETA: The Simplest ETA and also a Basic Action Unit.** The simplest ETA is a U-shaped actuator. Considering the anisotropy of BP material, there are two ways to cut the U-shaped BP electrode, vertically and horizontally, as shown in Figure 2a. Correspondingly, the CNT-aligned direction is parallel to the length direction of the vertically cut U-shaped electrode and perpendicular to the length direction of the horizontally cut electrode. The prepared actuators have two layers, one is the BP layer and the other is the PDMS layer. Comparing the actuations of the two ETAs, shown in Figure 2b,c and video S2 (Supporting Information), we had two observations. First, the two ETAs bent to the BP sides along the length direction of the U-shaped electrodes, and the deformation of the horizontally cut actuator (Figure 2c) was much larger, where the CNT alignment was perpendicular to the U-shaped BP band. Second, the parts which generated more heat would show obvious bending in the two ETAs. These parts also had larger electrical resistances.

The explanations of the bending are as follows. When the double-layer composite film is electrically heated, the fast temperature increase will cause thermal expansion. Since the BP and PDMS materials have significant difference in CTE,[38−40] that is, the $\alpha_{CNT} = 3 \times 10^{-6}$ K$^{-1}$ is two magnitudes smaller than $\alpha_{PDMS} = 3.1 \times 10^{-4}$ K$^{-1}$, there will be great thermal expansion mismatch between the two materials, which leads to obvious bending toward the BP side, as shown in Figure 2d. The bending angle can be described as $\theta = c \times \alpha_{2,1} \times \Delta T \times (L/d)$, where $\alpha_{2,1}$ is the CTE difference of the two materials, $c$ is a constant ($2 < c < 3$), and the film thickness $d$ in the range of 300−500 $\mu$m is appropriate. The detailed derivation process is shown in part 1 of the Supporting Information. Strictly speaking, it is more accurate to use the thickness of the PDMS layer $d_{PDMS}$ in the bending angle formula, but since the BP thickness $d_{BP}$ is in a narrow range (40 $\mu$m ∼ 50 $\mu$m), it can be seen as a constant. The thickness ratio $\eta = d_{PDMS}/d_{BP}$ is about 7−12, so normally we use the total thickness $d = d_{PDMS} + d_{BP}$ in the bending angle formula. In addition, there is a one-to-one correspondence relationship between total thickness $d$ and thickness ratio $\eta$, and the two variables are equal in

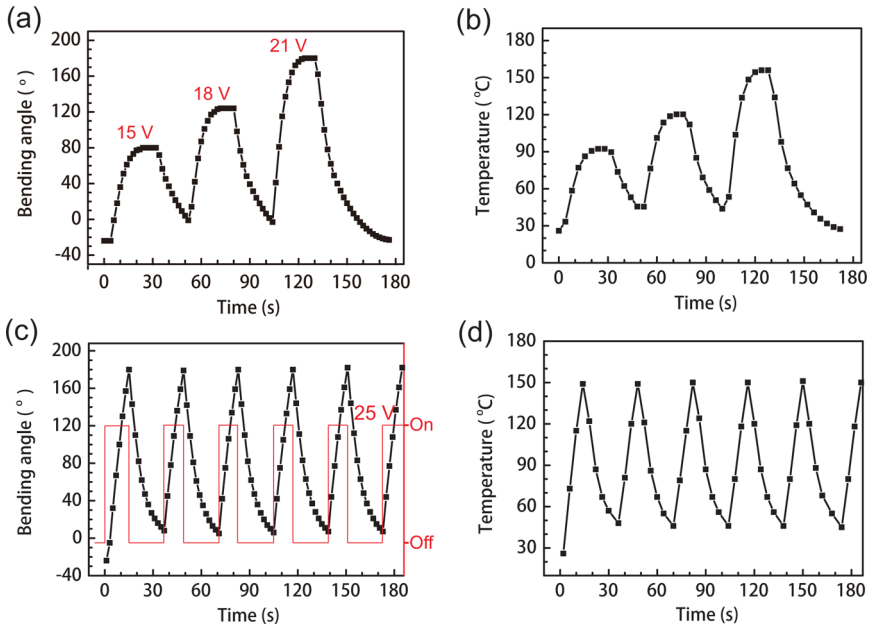


**Figure 3. (a) Bending angle of the U-shaped ETA varied as a function of time, under different driving voltage (15, 18, and 21 V). The maximum bending angle increases with the voltage. (b) The temperature change versus time, corresponding to (a). (c, d) Cyclic actuations and corresponding temperature change of the U-shaped ETA driven by a 25 V square wave.**

affecting the bending angles (relevant discussions are in part 2 of the Supporting Information). Because it is much easier to measure total thickness than $\eta$, we prefer to use $d$ in evaluating performances of the actuators. Generally, $\alpha_{2,1}$ and $d$ are determined. In order to obtain large bending, we should increase the temperature $\Delta T$ and the length of the BP electrode $L$. Thus, the long BP strip with larger resistance which is usually perpendicular (or inclined) to the CNT-aligned direction will have a larger temperature increase and show obvious bending when electrically heated. Therefore, in practical applications, we prefer the horizontally cut U-shaped ETA (shown in Figure 2c) where the CNT alignment is perpendicular to the length direction of the U-shaped electrode and it could bend to 180° when driven by electricity (25 V, 0.17 A).

Figure 3a shows that the maximum bending angles of the U-shaped ETA (in Figure 2c) varies with different driving voltages (15, 18 and 21 V). The deformation of the actuator would get larger when the voltage was higher. It is also found that, under a certain driving voltage, the bending speed was the fastest in the first seconds of turning on the power, and then the actuation slowed down, and finally, the actuator reached its maximum bending angle. Figure 3b is the temperature change of the U-shaped ETA which corresponds to Figure 3a. The bending speed, or response speed, is mainly determined by the speed of the temperature change. At first without current driving, the temperature of the actuator was equal to the room temperature. Once the power was turned on, a fast temperature increase caused a quick response. When the temperature was higher, the air convection was stronger and caused severe heat loss and a slower response speed. When the heat loss gradually got stronger and finally was equal to the generated heat, the temperature stabilized at the highest point, and the actuator also reached its maximum deformation. On the basis of the same principle, the temperature drop and the recovery speed of the actuator were the fastest in the first seconds of turning off the power and then slowed down gradually when the temperature got lower.

Parts c and d of Figure 3 show the movement cycles and corresponding temperature change of the U-shaped ETA driven by a 25 V square wave. It took the ETA only 12 s to bend from 0° to 180°, and the recovery process cost about 22 s. Higher driving voltage leads to faster bending motion. Thus, the CNT−PDMS double-layer ETA has the advantages of fast response speed in achieving large-strain deformations compared to other reported ETAs[19,21,41] and of low driving voltage compared to the field-driven EAPs. In addition, the highest working temperature was about150 °C, which is much less than250 °C, the maximum service temperature of PDMS.[37] This could ensure the ETA has a long service life.

The U-shaped actuator is the simplest ETA and also is the basic action unit. Based on the large-area BP materials, we could design various complex ETAs by assembling or integrating the U-shaped units and realize various functional or interesting actuations.

**T-Shaped ETA: Three Different Action Forms.** Figure 4a shows the typical design of a T-shaped ETA which is a little more complex. There are three different directions to cut the T-shaped electrode on BP, vertically, horizontally, and 45° inclined, as shown in Figure 4b.

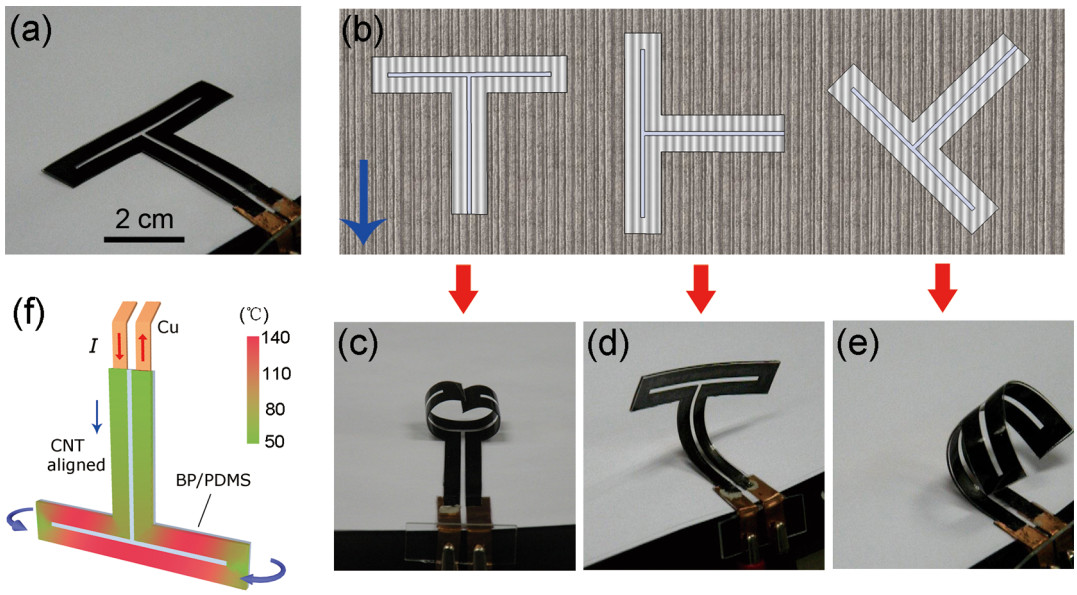


**Figure 4. Actuations of the T-shaped actuators. (a) As-prepared T-shaped actuator before current heating. (b) Three different ways of processing T-shaped BP electrodes: vertically, horizontally, and diagonally. The blue arrow indicates the CNT-aligned direction. (c−e) Actuations of the three T-shaped ETAs with different CNT alignment, which correspond to three different cutting modes on BP electrodes in (b). (f) Schematic of temperature distribution of the vertically cut ETA under current heating. The temperature is measured by Optris LS infrared thermometer (temperature resolution: 0.1 K; spatial resolution: 1 mm). The strips with larger resistances are much hotter than other parts, which results in obvious horizontal bending.**

It is interesting that the three T-shaped actuators showed different action forms when electrically heated (24−30 V, 0.18−0.25 A), as shown in Figure 4c−e and video S3 (Supporting Information). We wondered why. The reason is they have different CNT alignments that lead to different temperature distributions. Figure 4f shows the temperature distribution of the vertically cut ETA in Figure 4c. The two horizontal bars were obviously hotter than other parts, which resulted in large horizontal bending, whereas the vertical stem hardly bent. Similarly, for the horizontally cut T-shaped ETA (Figure 4d), the vertical stem was hotter and bent obviously. As for the diagonally cut ETA (Figure 4e), the inclined cutting caused uniform heating and isotropic bendings. Thus, we conclude that the anisotropy of BP can largely regulate the action forms of the ETAs. However, the three actuators have common action rules; that is, obvious deformations appear at the long BP bands which have larger resistances. In other words, a large temperature rise and long electrode configuration will lead to obvious bending. Based on these rules, we can further fabricate various novel ETAs and realize multiform actuations by virtue of complex electrode design and the anisotropy of BP.

**Performances of the T-Shaped ETAs.** The T-shaped ETA is a typical design of which the performances and key parameters could be the reference for other complex ETAs. We take the vertically cut T-shaped actuator (Figure 4c) as an example.

First is the response speed of the movement which is mainly influenced by driving current and the thickness of the composite film. It was found that the response time decreased with driving current and increased with the film thickness, which corresponded to the thermal capacity, as shown in Figure 5a,b. Evidently, the driving current and film thickness determine the temperature rise and drop rate and further determine the response speed. Generally, it takes a 300-$\mu$m-thick actuator 10 s to accomplish 180° bending motion driven by the current of 0.12 A.

Second, the maximum bending angle was determined as a function of driving current, and the relationship was approximately linear from 0.03 to 0.15 A, as shown in Figure 5c. The maximum bending angle means the largest deformations that an actuator could achieve under the driving of a certain size of voltage or current. Like the motions of the U-shaped ETA described in Figure 3a, the T-shaped ETA bent quickly when the power was turned on, and then the bending speed gradually slowed down. Finally, the bending deformation stopped at a certain angle (maximum angle). At that moment, if we turned up the driving voltage slightly, the maximum bending angle would get a little larger. Thus, the precise control of the bending angle is feasible in a wide range, from −100° to +190°, by means of fine-tuning of the driving voltage or current. If the thermal radiation does not play a role in thermal dissipation, the maximum bending angle (or the temperature rise) should be proportional to the square of current (*i.e.*, Joule heating), but when the ETAs get hotter, the thermal radiation will cause the temperature increase to be obviously lower than that without radiation and make the relationship between $\theta$ and $I$ highly nonlinear. Therefore, the

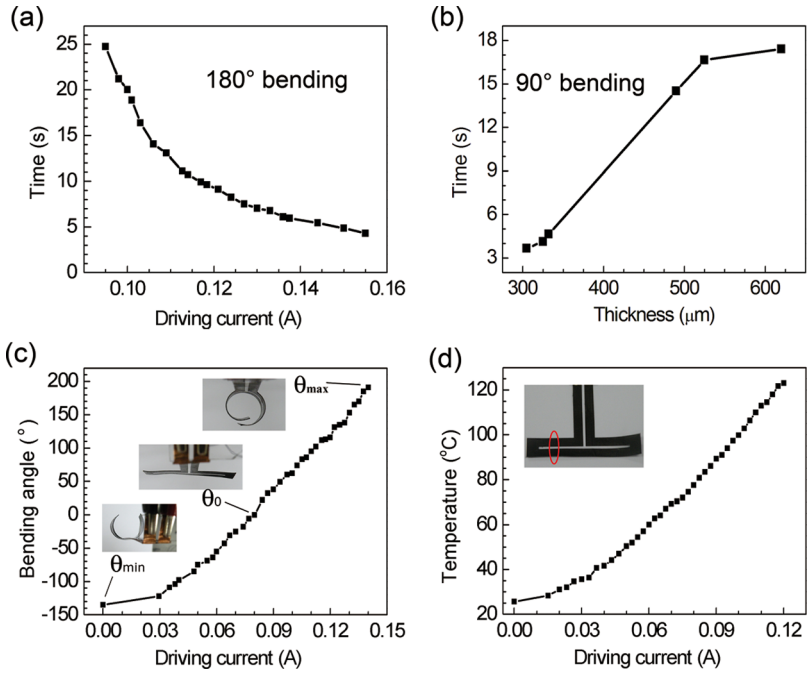


**Figure 5. Performances and key parameters of the vertically cut T-shaped ETA. (a) Actuation time of achieving 180° bending as a function of driving current. (b) Actuation time of achieving 90° bending as a function of the thickness of the composite film under a certain current (0.13 A) driving. (c) The maximum bending angle varies with driving current. The three insets correspond to $\theta_{min}$, $\theta_0$, and $\theta_{max}$, respectively. (d) The maximum working temperature as a function of driving current. Inset: the red circle indicates the temperature measuring area. The thickness of the ETA is 305 $\mu$m in (a), (c), and (d).**

approximate linear relationship between $\theta$ and $I$ is just an empirical result, not theoretical. A detailed discussion is included in part 3 of the Supporting Information.

Third, it was also found that the working temperature increased with driving current, as shown in Figure 5d. The normal working temperature of the ETA was below 150 °C, which was much less than the maximum service temperature of PDMS 250 °C. This could ensure long service life of the ETAs. Over 10000 action cycles have been verified for the T-shaped ETA.

A finite element analysis (FEA) was carried out to simulate the actuations and temperature distributions of the T-shaped ETA through commercial FEA software ABAQUS. The simulation results (shown in Figure 6a) were also used for comparison with the experimental results. Figure 6b is the initial state of the T-shaped ETA, which is flat and was prepared under the 80 °C conditions. When the ETA was brought out from the vacuum drying oven and cooled to 25 °C, it would show obvious reverse bending (toward PDMS side), as shown in Figure 6c. Parts d−i of Figure 6 show the bending states and temperature distributions of the ETA, which was heated by different values of current. The corresponding bending angles are also marked in Figure 6a (red solid circles) and compared to the experimental data (cited from Figure 5c). We can see these two sets of results match well. The simulation details can be seen in the Supporting Information.

Fourth, the driving voltages of all ETAs are usually below 200 V, and the driving currents are less than 0.3 A. Thus, the ETAs are easy to drive and operate by common voltage-output equipment. Fifth, the output force of the U-shaped action unit is generally three times of its own weight (~0.25 g), so the as-prepared ETAs can lift certain things, such as foamed plastic balls. The maximum energy efficiency of the ETA is about 0.003%, for much Joule heating dissipates into the environment. On the whole, the above performances and key parameters make the ETAs competent for practical applications.

Until now, the design methods, actuation rules, and performance of the U-shaped and T-shaped ETAs have been clear. On these bases, we can carry out complex electrode designs on large-area BP and fabricate functional or interesting ETAs. Next are several application examples.

**Complex Design: Z-Shaped ETA, an Interesting Application.** The Z-shaped actuator is much more complex (inset in Figure 7a). The electrode was well designed to form a zigzag series circuit, and the diagonal bands inclined to the CNT alignment (indicated by the blue arrow) at an angle of 45°. When electrically heated (160 V, 0.3 A), the actuator helically curled up, reached the maximum angle of 630°, and then unfolded when the power was off, as shown in Figure 7a and video S4 (Supporting Information). The diagonal BP bands with larger resistances bent obviously which once again proved the actuation rules. The highly anisotropic property of BP material plays an important role in the complex and functional design of the actuators. If the Z-shaped ETA

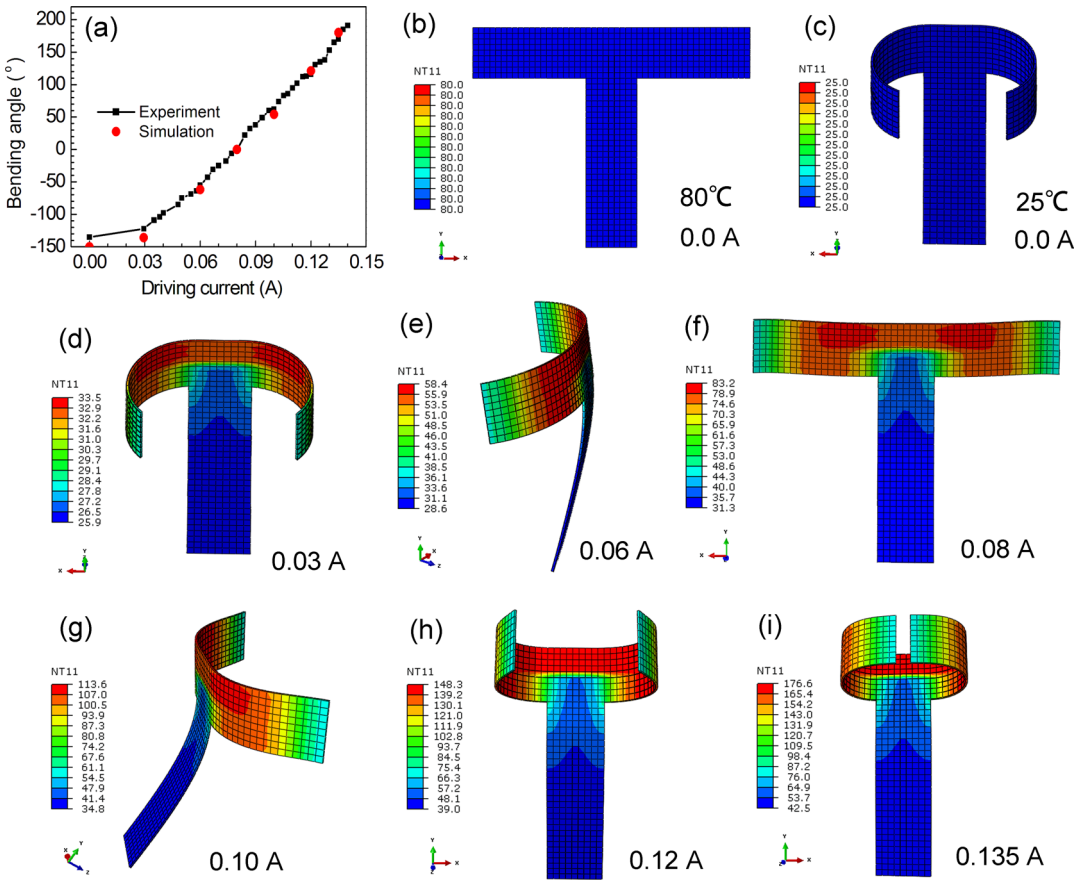


**Figure 6. FEA simulations on the bending states of the T-shaped actuator. (a) FEA simulations of bending angle vs driving current (red solid circles) were compared to the experiment data (cited from Figure 5c). (b) State just after the actuator was prepared in 80 °C. The actuator was flat (Initial state). (c) Actuator was cooled down to 25 °C (ambient temperature) and bent toward PDMS side without current driving. (d−i) The bending states of the actuator which was heated by a certain current (0.03, 0.06, 0.08, 0.10, 0.12, 0.135 A, respectively). NT11 means "nodal temperature at nodes"; the field output in color shows the temperature distribution of the actuator.**

was based on an isotropic electrode material, it could not realize the actuation of helical curling. In that case, all of the bands would bend, and there would not be selective bending. Thus, it is concluded that the anisotropy of BP can influence the action form significantly and the anisotropy is the most outstanding property of the BP material.

**Bionic Design: Hand-Shaped Actuators.** Another interesting design is the hand-shaped actuator shown in Figure 7b. The BP electrode was designed as the shape of a human hand. It is a series circuit. The CNT-aligned direction is perpendicular to the forefinger. The thumb inclines to the forefinger at an angle of 30°. When electrically heated (200 V, 0.23 A), the five fingers all bent inward and then unfolded when power was off, as shown in Figure 7c and video S5 (Supporting Information). Figure 7d shows the bending angles of the five fingers vary as a function of time. It took the five fingers 12 s to achieve the maximum angles (the four parallel fingers can bend more than 180°, the thumb can bend to 120°), and then it took the fingers 28 s to restore their original shapes. The whole movement vividly imitated the grabbing and spreading actions of a man's hand without the help of any mechanical devices.

Furthermore, we also designed and fabricated a more complex hand-shaped actuator which realized separate movements of the five fingers controlled by five independent circuits. Each finger could move separately (Figure 8a−c), so the actuator could perform various gestures as shown in Figure 8d−f and video S6 (Supporting Information).

The artful electrode design and the anisotropy of BP both played significant roles in preparing complex ETAs and in realizing novel, functional actuations. This interesting work is also based on the efficient preparation of large-area BP electrodes and convenient processing.

In addition to the CNT-based ETA, there is another class of bimorph ETAs based on graphene.[42−44] Graphene has intrinsic negative CTE (~$-10^{-6}$),[45] and it could be used for making bimorph microactuator.[42,43] Some graphene oxide or spongy graphene paper has much larger negative CTE value (~$-10^{-4}$),[46,47] so the graphene−polymer bilayer ETAs could accomplish large-stain bending under a smaller temperature

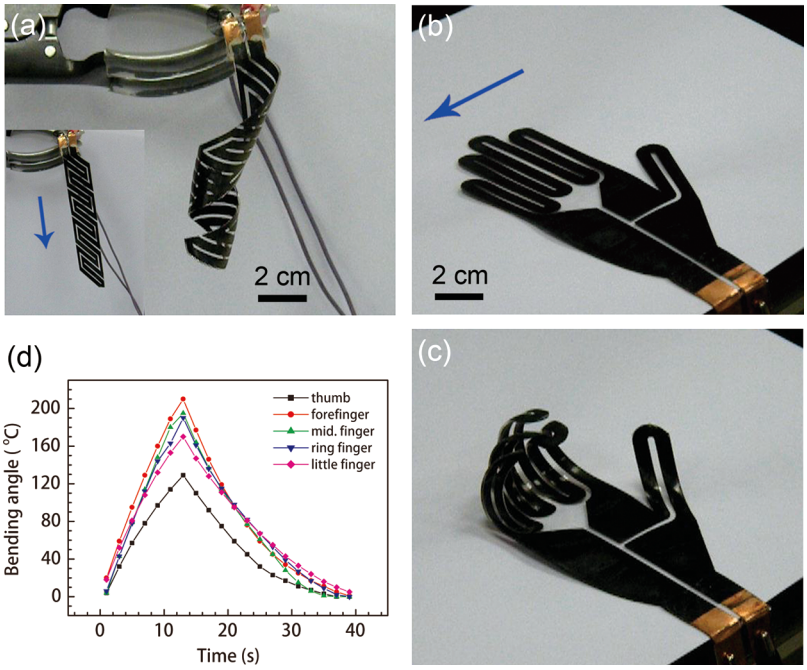


**Figure 7. (a) Actuation of the Z-shaped actuator. Inset: original shape of the actuator. (b, c) Original shape and corresponding actuation of the hand-shaped actuator. (d) Bending angles of the five fingers vary as functions of time for the hand-shaped actuator.**

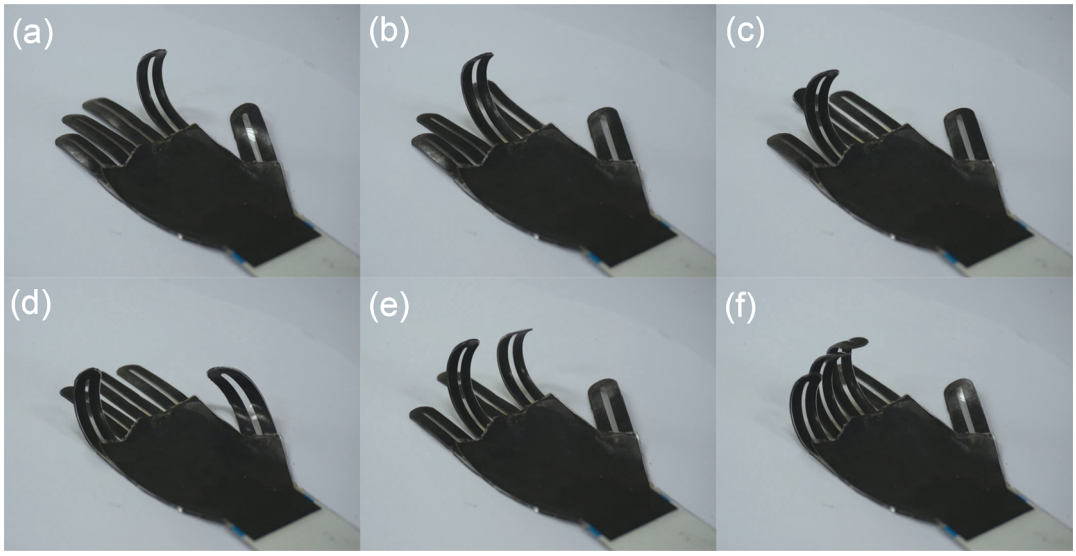


**Figure 8. Actuations of the improved hand-shaped ETA. (a–c) Independent control of forefinger, middle finger, and ring finger. (d–f) Various gestures that the ETA could make.**

rise compared to the CNT–polymer ETAs.[44] However, the CNT-based actuator has its own advantages: (i) the CNT electrode could be prepared efficiently through dry methods and in very large area; (ii) the electrode made of aligned CNTs will show highly anisotropic properties; and (iii) the large-area CNT electrode could be designed and processed to functional patterns for multiform actuations. Thus, the CNT- and graphene-based ETAs have their own advantages and could complement each other well in practical applications.

## CONCLUSIONS

In summary, we have developed new ETAs which can realize multiform actions or bionic actuations based on large-area CNT-based electrodes. Owing to the significant thermal expansion difference between BP and PDMS, the ETAs can achieve large-strain deformations. By virtue of novel design and fine processing on the anisotropic BP electrode, the ETAs can realize various functional movements according to demand. The ETAs are low-voltage driven and electrolyte free.

In addition, the mass production of large-area BP electrodes and efficient processing are also feasible. Therefore, the ETAs can be flexibly designed and widely used in flexible actuation field, multiform deformations or displays, or even bionic robot fields.

## METHODS

**Graphic Design and Laser Cutting on BP.** Graphics software has been employed to design functional patterns, for example, a T-shaped band. The pattern information was transferred to the control unit of laser control equipment, and the laser cutting was carried out on the as-prepared BP to get this conductive band, shown in Figure 1d. The graphic design of electrodes is very flexible, and the laser cutting process is also efficient and of high precision (0.2 mm). Thus, various complex BP electrodes can be fabricated easily, and the corresponding prepared ETAs can realize various interesting deformations or actuations.

**Preparation of BP–PDMS Double-Layer ETA.** The as-prepared BP band (40–50 $\mu$m thick) was spread on a flat polystyrene (PS) board. A small amount of silver colloid was dropped on the ends of the conductive band, and two copper sheets were stuck on them. Next, the dimethylsiloxane (DMS) mixture (SG3010 component A and B, 1:1 by weight, from Beijing Hangtongzhou Technology Co., Ltd.) was poured on the whole device. It was then put in a vacuum drying oven, heated to 80 °C, and maintained for 4 h. After DMS solidified, the whole composite film could peeled off completely from the PS board, and finally the CNT-PDMS ETA was cut out along the outline of BP pattern. The above process is demonstrated in video S1 (Supporting Information). The as-prepared ETA is a double-layer composite film, about 300–500 $\mu$m thick. The film thickness can be regulated by adjusting the DMS consumption in the preparation process.

*Conflict of Interest:* The authors declare no competing financial interest.

*Acknowledgment.* This work was financially supported by National Basic Research Program of China (2012CB932301), Natural Science Foundation of China (51173098), and China Postdoctoral Science Foundation (023200006).

*Supporting Information Available:* Derivations of the bending angle formula, discussion about thickness ratio of the two layers, discussion about the relationship between maximum bending angle and driving current, and finite element simulations on bending states are shown. Additional videos are described in the text (videos S1–S6). This material is available free of charge *via* the Internet at http://pubs.acs.org.

## REFERENCES AND NOTES

1. Mirfakhrai, T.; Madden, J.; Baughman, R. H. Polymer Artificial Muscles. *Mater. Today* **2007**, *10*, 30–38.
2. Bar-Cohen, Y. *Electroactive Polymer (EAP) Actuators as Artificial Muscles: Reality, Potential, and Challenges*; SPIE Press: Bellingham, WA, 2004.
3. Madden, J. D. W.; Vandesteeg, N. A.; Anquetil, P. A.; Madden, P.; Takshi, A.; Pytel, R. Z.; Lafontaine, S. R.; Wieringa, P. A.; Hunter, I. W. Artificial Muscle Technology: Physical Principles and Naval Prospects. *IEEE J. Oceanic Eng.* **2004**, *29*, 706–728.
4. Brochu, P.; Pei, Q. B. Advances in Dielectric Elastomers for Actuators and Artificial Muscles. *Macromol. Rapid Commun.* **2010**, *31*, 10–36.
5. Subramani, K. B.; Cakmak, E.; Spontak, R. J.; Ghosh, T. K. Enhanced Electroactive Response of Unidirectional Elastomeric Composites with High-Dielectric-Constant Fibers. *Adv. Mater.* **2014**, *26*, 2949–2953.
6. Wu, J. H.; Zang, J. F.; Rathmell, A. R.; Zhao, X. H.; Wiley, B. J. Reversible Sliding in Networks of Nanowires. *Nano Lett.* **2013**, *13*, 2381–2386.
7. Pelrine, R.; Kornbluh, R.; Pei, Q. B.; Joseph, J. High-Speed Electrically Actuated Elastomers with Strain Greater than 100%. *Science* **2000**, *287*, 836–839.
8. Zhang, Q. M.; Bharti, V.; Zhao, X. Giant Electrostriction and Relaxor Ferroelectric Behavior in Electron-Irradiated Poly(vinylidene fluoride-trifluoroethylene) Copolymer. *Science* **1998**, *280*, 2101–2104.
9. Lehmann, W.; Skupin, H.; Tolksdorf, C.; Gebhard, E.; Zentel, R.; Kruger, P.; Losche, M.; Kremer, F. Giant Lateral Electrostriction in Ferroelectric Liquid-Crystalline Elastomers. *Nature* **2001**, *410*, 447–450.
10. Baughman, R. H.; Cui, C. X.; Zakhidov, A. A.; Iqbal, Z.; Barisci, J. N.; Spinks, G. M.; Wallace, G. G.; Mazzoldi, A.; De Rossi, D.; Rinzler, A. G.; *et al.* Carbon Nanotube Actuators. *Science* **1999**, *284*, 1340–1344.
11. Xie, X. J.; Qu, L. T.; Zhou, C.; Li, Y.; Zhu, J.; Bai, H.; Shi, G. Q.; Dai, L. M. An Asymmetrically Surface-Modified Graphene Film Electrochemical Actuator. *ACS Nano* **2010**, *4*, 6050–6054.
12. Kim, O.; Shin, T. J.; Park, M. J. Fast Low-Voltage Electroactive Actuators Using Nanostructured Polymer Electrolytes. *Nat. Commun.* **2013**, *4*, 2208.
13. Kim, J.; Jeon, J. H.; Kim, H. J.; Lim, H.; Oh, I. K. Durable and Water-Floatable Ionic Polymer Actuator with Hydrophobic and Asymmetrically Laser-Scribed Reduced Graphene Oxide Paper Electrodes. *ACS Nano* **2014**, *8*, 2986–2997.
14. Rajagopalan, M.; Oh, I. K. Fullerenol-Based Electroactive Artificial Muscles Utilizing Biocompatible Polyetherimide. *ACS Nano* **2011**, *5*, 2248–2256.
15. Chen, L. Z.; Liu, C. H.; Hu, C. H.; Fan, S. S. Electrothermal Actuation Based on Carbon Nanotube Network in Silicone Elastomer. *Appl. Phys. Lett.* **2008**, *92*, 263104.
16. Sellinger, A. T.; Wang, D. H.; Tan, L. S.; Vaia, R. A. Electrothermal Polymer Nanocomposite Actuators. *Adv. Mater.* **2010**, *22*, 3430–3435.
17. Hu, Y.; Chen, W.; Lu, L. H.; Liu, J. H.; Chang, C. R. Electromechanical Actuation with Controllable Motion Based on a Single-Walled Carbon Nanotube and Natural Biopolymer Composite. *ACS Nano* **2010**, *4*, 3498–3502.
18. Chen, L. Z.; Liu, C. H.; Liu, K.; Meng, C. Z.; Hu, C. H.; Wang, J. P.; Fan, S. S. High-Performance, Low-Voltage, and Easy-Operable Bending Actuator Based on Aligned Carbon Nanotube/Polymer Composites. *ACS Nano* **2011**, *5*, 1588–1593.
19. Seo, D. K.; Kang, T. J.; Kim, D. W.; Kim, Y. H. Twistable and Bendable Actuator: a CNT/Polymer Sandwich Structure Driven by Thermal Gradient. *Nanotechnology* **2012**, *23*, 75501.
20. Liang, J. J.; Huang, L.; Li, N.; Huang, Y.; Wu, Y. P.; Fang, S. L.; Oh, J.; Kozlov, M.; Ma, Y. F.; Li, F. F.; *et al.* Electromechanical Actuator with Controllable Motion, Fast Response Rate, and High-Frequency Resonance Based on Graphene and Polydiacetylene. *ACS Nano* **2012**, *6*, 4508–4519.
21. Zhang, X. B.; Pint, C. L.; Lee, M. H.; Schubert, B. E.; Jamshidi, A.; Takei, K.; Ko, H.; Gillies, A.; Bardhan, R.; Urban, J. J.; *et al.* Optically- and Thermally-Responsive Programmable Materials Based on Carbon Nanotube-Hydrogel Polymer Composites. *Nano Lett.* **2011**, *11*, 3239–3244.
22. Zhang, X.; Yu, Z. B.; Wang, C.; Zarrouk, D.; Seo, J.; Cheng, J. C.; Buchan, A. D.; Takei, K.; Zhao, Y.; Ager, J. W.; *et al.* Photoactuators and Motors Based on Carbon Nanotubes with Selective Chirality Distributions. *Nat. Commun.* **2014**, *5*, 2983.
23. Ebbesen, T. W.; Lezec, H. J.; Hiura, H.; Bennett, J. W.; Ghaemi, H. F.; Thio, T. Electrical Conductivity of Individual Carbon Nanotubes. *Nature* **1996**, *382*, 54–56.
24. Falvo, M. R.; Clary, G. J.; Taylor, R. M.; Chi, V.; Brooks, F. P.; Washburn, S. Superfine, R. Bending and Buckling of Carbon Nanotubes under Large Strain. *Nature* **1997**, *389*, 582–584.

25. Kim, Y. A.; Muramatsu, H.; Hayashi, T.; Endo, M.; Terrones, M.; Dresselhaus, M. S. Thermal Stability and Structural Changes of Double-Walled Carbon Nanotubes by Heat Treatment. *Chem. Phys. Lett.* **2004**, *398*, 87–92.
26. Sun, C. Q.; Bai, H. L.; Tay, B. K.; Li, S.; Jiang, E. Y. Dimension, Strength, and Chemical and Thermal Stability of a Single C-C Bond in Carbon Nanotubes. *J. Phys. Chem. B* **2003**, *107*, 7544–7546.
27. Inam, F.; Yan, H.; Reece, M. J.; Peijs, T. Structural and Chemical Stability of Multiwall Carbon Nanotubes in Sintered Ceramic Nanocomposite. *Adv. Appl. Ceram.* **2010**, *109*, 240–245.
28. Lima, M. D.; Li, N.; de Andrade, M. J.; Fang, S. L.; Oh, J.; Spinks, G. M.; Kozlov, M. E.; Haines, C. S.; Suh, D.; Foroughi, J.; *et al.* Electrically, Chemically, and Photonically Powered Torsional and Tensile Actuation of Hybrid Carbon Nanotube Yarn Muscles. *Science* **2012**, *338*, 928–932.
29. Foroughi, J.; Spinks, G. M.; Wallace, G. G.; Oh, J.; Kozlov, M. E.; Fang, S. L.; Mirfakhrai, T.; Madden, J.; Shin, M. K.; Kim, S. J.; *et al.* Torsional Carbon Nanotube Artificial Muscles. *Science* **2011**, *334*, 494–497.
30. Aliev, A. E.; Oh, J. Y.; Kozlov, M. E.; Kuznetsov, A. A.; Fang, S. L.; Fonseca, A. F.; Ovalle, R.; Lima, M. D.; Haque, M. H.; Gartstein, Y. N.; *et al.* Giant-Stroke, Superelastic Carbon Nanotube Aerogel Muscles. *Science* **2009**, *323*, 1575–1578.
31. Guo, W. H.; Liu, C.; Zhao, F. Y.; Sun, X. M.; Yang, Z. B.; Chen, T.; Chen, X. L.; Qiu, L. B.; Hu, X. H.; Peng, H. S. A Novel Electromechanical Actuation Mechanism of a Carbon Nanotube Fiber. *Adv. Mater.* **2012**, *24*, 5379–5384.
32. Li, J. Z.; Ma, W. J.; Song, L.; Niu, Z. G.; Cai, L.; Zeng, Q. S.; Zhang, X. X.; Dong, H. B.; Zhao, D.; Zhou, W. Y.; *et al.* Superfast-Response and Ultrahigh-Power-Density Electromechanical Actuators Based on Hierarchal Carbon Nanotube Electrodes and Chitosan. *Nano Lett.* **2011**, *11*, 4636–4641.
33. Fan, S. S.; Chapline, M. G.; Franklin, N. R.; Tombler, T. W.; Cassell, A. M.; Dai, H. J. Self-Oriented Regular Arrays of Carbon Nanotubes and Their Field Emission Properties. *Science* **1999**, *283*, 512–514.
34. Jiang, K. L.; Li, Q. Q.; Fan, S. S. Nanotechnology: Spinning Continuous Carbon Nanotube Yarns - Carbon Nanotubes Weave Their Way into a Range of Imaginative Macroscopic Applications. *Nature* **2002**, *419*, 801.
35. Zhang, X. B.; Jiang, K. L.; Teng, C.; Liu, P.; Zhang, L.; Kong, J.; Zhang, T. H.; Li, Q. Q.; Fan, S. S. Spinning and Processing Continuous Yarns from 4-Inch Wafer Scale Super-Aligned Carbon Nanotube Arrays. *Adv. Mater.* **2006**, *18*, 1505.
36. Jiang, K. L.; Wang, J. P.; Li, Q. Q.; Liu, L. A.; Liu, C. H.; Fan, S. S. Superaligned Carbon Nanotube Arrays, Films, and Yarns: A Road to Applications. *Adv. Mater.* **2011**, *23*, 1154–1161.
37. Liu, M.; Sun, J. R.; Chen, Q. F. Influences of Heating Temperature on Mechanical Properties of Polydimethylsiloxane. *Sens. Actuator, A* **2009**, *151*, 42–45.
38. Lin, Y. H.; Kang, S. W.; Wu, T. Y. Fabrication of Polydimethylsiloxane (PDMS) Pulsating Heat Pipe. *Appl. Therm. Eng.* **2009**, *29*, 573–580.
39. Schelling, P. K.; Keblinski, R. Thermal Expansion of Carbon Structures. *Phys. Rev. B* **2003**, *68*, 35425.
40. Li, C. Y.; Chou, T. W. Axial and Radial Thermal Expansions of Single-Walled Carbon Nanotubes. *Phys. Rev. B* **2005**, *71*, 235414.
41. Yu, C. J.; Duan, Z.; Yuan, P. X.; Li, Y. H.; Su, Y. W.; Zhang, X.; Pan, Y. P.; Dai, L. L.; Nuzzo, R. G.; Huang, Y. G.; *et al.* Electronically Programmable, Reversible Shape Change in Two- and Three-Dimensional Hydrogel Structures. *Adv. Mater.* **2013**, *25*, 1541–1546.
42. Zhu, S.; Shabani, R.; Rho, J.; Kim, Y.; Hong, B. H.; Ahn, J.; Cho, H. J. Graphene-Based Bimorph Microactuators. *Nano Lett.* **2011**, *11*, 977–981.
43. Conley, H.; Lavrik, N. V.; Prasai, D.; Bolotin, K. I. Graphene Bimetallic-Like Cantilevers: Probing Graphene/Substrate Interactions. *Nano Lett.* **2011**, *11*, 4748–4752.
44. Hu, Y.; Lan, T.; Wu, G.; Zhu, Z.; Chen, W. A Spongy Graphene Based Bimorph Actuator with Ultra-Large Displacement Towards Biomimetic Application. *Nanoscale* **2014**, *6*, 12703–12709.
45. Yoon, D.; Son, Y. W.; Cheong, H. Negative Thermal Expansion Coefficient of Graphene Measured by Raman Spectroscopy. *Nano Lett.* **2011**, *11*, 3227–3231.
46. Zhu, J.; Andres, C. M.; Xu, J. D.; Ramamoorthy, A.; Tsotsis, T.; Kotov, N. A. Pseudonegative Thermal Expansion and the State of Water in Graphene Oxide Layered Assemblies. *ACS Nano* **2012**, *6*, 8357–8365.
47. Hu, Y.; Lan, T.; Wu, G.; Zhu, Z. C.; Tao, X. M.; Chen, W. Novel Electromechanical Actuation Based On a Spongy Graphene Paper. *Chem. Commun.* **2014**, *50*, 4951–4954.